Journal of Microscopy, Vol. 230, Pt 1 2008, pp. 143–159
Received 4 April 2007; accepted 2 October 2007

A statistical approach for intensity loss compensation of confocal microscopy images

S. GOPINATH*, Q. WEN*, N. THAKOOR† , K. LUBY-PHELPS‡ & J. X. GAO§
*Computer Science and Engineering Department, University of Texas at Arlington, U.S.A.
†Electrical Engineering Department, University of Texas at Arlington, U.S.A.
‡Cell Biology Department, University of Texas Southwestern Medical Center, Dallas, TX, U.S.A.
§Computer Science and Engineering Department, University of Texas at Arlington, U.S.A.

Key words. Compensation, confocal microscopy, expectation maximization, intensity loss, photobleaching.

Summary

In this paper, a probabilistic technique for compensation of intensity loss in confocal microscopy images is presented. For single-colour-labelled specimen, confocal microscopy images are modelled as a mixture of two Gaussian probability distribution functions, one representing the background and another corresponding to the foreground. Images are segmented into foreground and background by applying Expectation Maximization algorithm to the mixture. Final intensity compensation is carried out by scaling and shifting the original intensities with the help of parameters estimated for the foreground. Since foreground is separated to calculate the compensation parameters, the method is effective even when image structure changes from frame to frame. As intensity decay function is not used, complexity associated with estimation of the intensity decay function parameters is eliminated. In addition, images can be compensated out of order, as only information from the reference image is required for the compensation of any image. These properties make our method an ideal tool for intensity compensation of confocal microscopy images that suffer intensity loss due to absorption/scattering of light as well as photobleaching and the image can change structure from optical/temporal section-to-section due to changes in the depth of specimen or due to a live specimen. The proposed method was tested with a number of confocal microscopy image stacks and results are presented to demonstrate the effectiveness of the method.

Correspondence to: Jean X. Gao. e-mail: gao@uta.edu

This work is supported in part by National Science Foundation NSF IIS-0546605, NSF IIS-0612152, NSF IIS-0612214.

Introduction

Images produced by confocal microscope tend to decrease in intensity with time as an effect of photobleaching when conventional fluorescence tags are used or with depth due to absorption or scattering of excitation and fluorescence. These effects make analysis of the images without intensity correction a complicated problem. Methods used to compensate the intensity loss can be categorized into two types,

- *Pre-processing methods*: Ones that correct the intensity loss with modified optics as the images are being captured (Atkins & De Paula, 1994; Chen *et al.*, 1995; Becker, 1996; Song *et al.*, 1996). More recently, a method, which manipulates the photomultiplier gain, was introduced to counter the high intensity losses in the deep layers of the specimen by Čapek *et al.* (2006).
- *Post-processing methods*: These methods compensate the images after they are captured (Rigaut & Vassy, 1991; Oostveldt *et al.*, 1998; Ortiz *et al.*, 1999; Kervrann *et al.*, 2004; Čapek *et al.*, 2005). Intensity decay function (IDF)–based methods model intensity loss in the images as a parametric decay function of depth or time. The decay parameters are estimated and compensated for in these methods. Another family of methods relies on matching histogram profiles of image stacks. These methods however cannot handle change in image structure along the optical axis.

Optics-based methods assume that the majority of the intensity loss is due to absorption and scattering of light as it travels through the specimen. As the rate of photobleaching can vary for different types of specimens, intensity loss cannot be ideally compensated by optics alone. For this reason, we concentrate on post-processing methods to correct the intensity loss.

As factors contributing to the intensity loss cannot be modelled accurately for practical images according to Wu & Ji (2005), it poses a problem when IDF is used for intensity compensation. In addition, the combination of intensity loss due to photobleaching and depth can give rise to a complicated IDF. Our method is motivated by histogram matching; however, it deals with a continuous domain by modelling an image as a mixture of two Gaussian probability distribution functions (PDFs) and matching the profiles of foreground probability distributions. By matching foreground and not the entire image, our method avoids the problems arising due to change in structure of the image. Different post-processing approaches to correct the intensity variations can be found in the literature. Negahdaripour & Yu (1993) apply a general model in which the horizontal and vertical flow fields as well as additive and multiplicative intensity relationships are estimated for every pixel. According to Ĉapek *et al.* (2005), this approach is computationally expensive. A least-squares optimization-based approach, which optimizes brightness and contrast, is proposed by Periaswamy & Farid (2003) and Kervrann *et al.* (2004). These techniques are highly sensitive to outliers. The reweighed least-squares method is used by Kervrann *et al.* (2004) to correct the disadvantage of Periaswamy & Farid (2003). The method discussed in Kervrann *et al.* (2004) is not only sensitive to noise which can be eliminated by median filtering but also to the dynamic movement of objects in neighbouring optical sections. According to Ĉapek *et al.* (2005), this gives erroneous and unstable results even in the presence of a very few outliers in optical sections. In Cox *et al.* (1995), intensity variations are corrected based on histogram warping, but it is restricted to the case where a global, spatially invariant, non-linear, monotonically increasing relationship exists between the intensities of the two images. Ĉapek *et al.* (2005) extend the approach of Cox *et al.* (1995) and attempt to give a general and fully automatic method of correcting intensity loss in confocal microscopy images. The proposed method manipulates the image histogram as in Ĉapek *et al.* (2005), but it focusses on the continuous domain of probabilities to filter the foreground information to calculate the correction parameters. Before we present our approach, we will discuss the approach by Ĉapek *et al.* (2005) in short. The approach proposed in Ĉapek *et al.* (2005) consists of two stages. In the first stage, a standard histogram is constructed with the help of histograms of all the optical sections in the image stack. In the second stage, individual histograms are warped according to the standard histogram to achieve the brightness and contrast of the standard histogram. The construction of standard histogram is adopted from Nyul *et al.* (2000). The approach is based on landmarks chosen in the image histogram. The landmarks chosen are the minimum and maximum intensities and percentiles of the intensities of the image. However, minimum and maximum intensity of image are highly sensitive to noise. For the images that change the structure from optical section-to-section, proportion of the foreground to the background varies. This causes substantial changes in histograms, making histogram-based methods less effective. The main idea of the proposed method is to filter the foreground information from a given image by modelling it as a mixture of Gaussian PDFs and use this information to compensate image intensity loss. The foreground mean and standard deviation are used to transform the pixel intensities of the original image relative to the intensity parameters of a reference image. The paper is organized as follows: Section 2 explains the proposed approach in detail. Section 3 presents experimental results. Paper concludes in Section 4.

Proposed approach

In many statistical applications, Gaussian mixture modelling (GMM) is used as a general tool for modelling a large heterogeneous population. Detailed introduction to GMM can be found in Theodoridis & Koutroumbas (1999). GMM is a semi-parametric estimation approach that provides good flexibility and precision in modelling the statistics of unlabelled sample data. In our case, the image data can be assumed to be generated from two components, one forming the

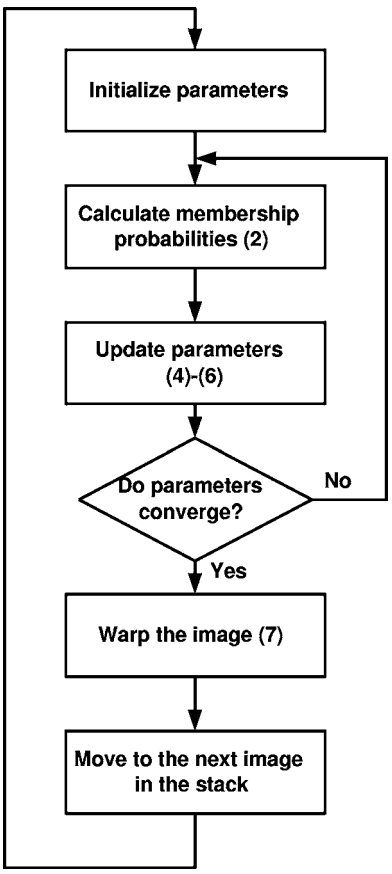

Fig. 1. Flowchart for the proposed compensation algorithm, numbers in the bracket indicate the corresponding equations.

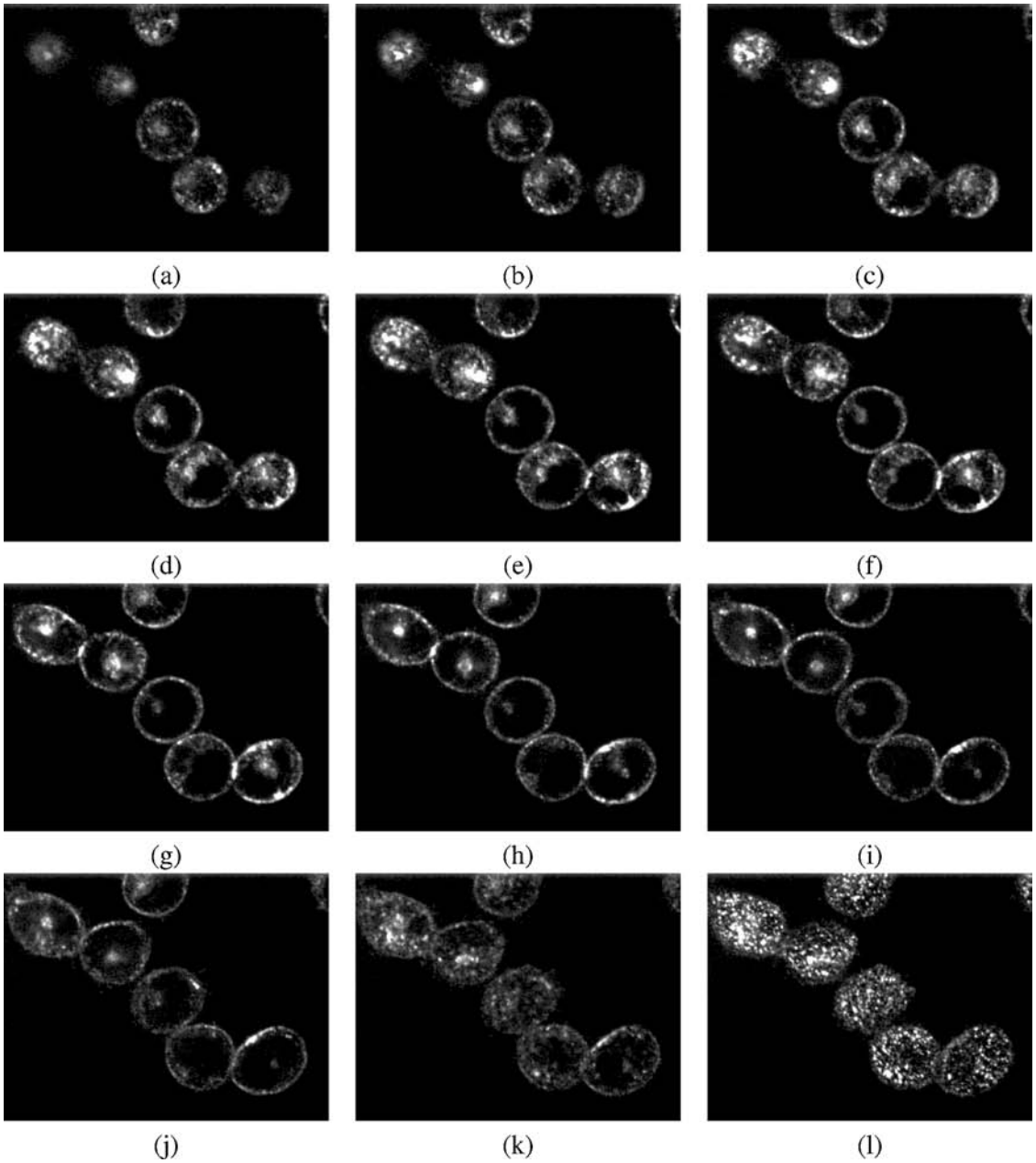

Fig. 2. Sequence 1: Original optical sections at time $t = 1$ from (a) top ($z = 1$) to (l) bottom ($z = 12$) (bottom frame is used as the reference).

background of the image and the other pertaining to the foreground of the image. However, it is not known that which pixel belongs to which component. Because of this, the problem can be considered to have missing data, that is, background/foreground membership information. Each component can be considered to have its own parameters θ, which define the probability density function $P_i(x;\theta)$. These parameters can be estimated through the expectation maximization (EM) algorithm, which is the widely used approach to solve the missing data problem. It devises appropriate parameters for the chosen model with respect to the data points generated by individual components. In the EM algorithm, initial estimates for the parameters are chosen arbitrarily. As the selection of initial estimates affects the result, they must be chosen carefully. The iterative parameter estimation process consists of two steps, the expectation (E) step and the maximization (M) step. In the E step, the expected value of the missing data is calculated. In the M step, the resulting value of the expectation is maximized by selecting new set of parameters. The E and M steps are iterated until a stopping criterion such as a number of iterations is met or until there is no change in the mixture model parameters. Most of the images captured with confocal microscopy are bimodal, one mode each for background and foreground. Hence, the

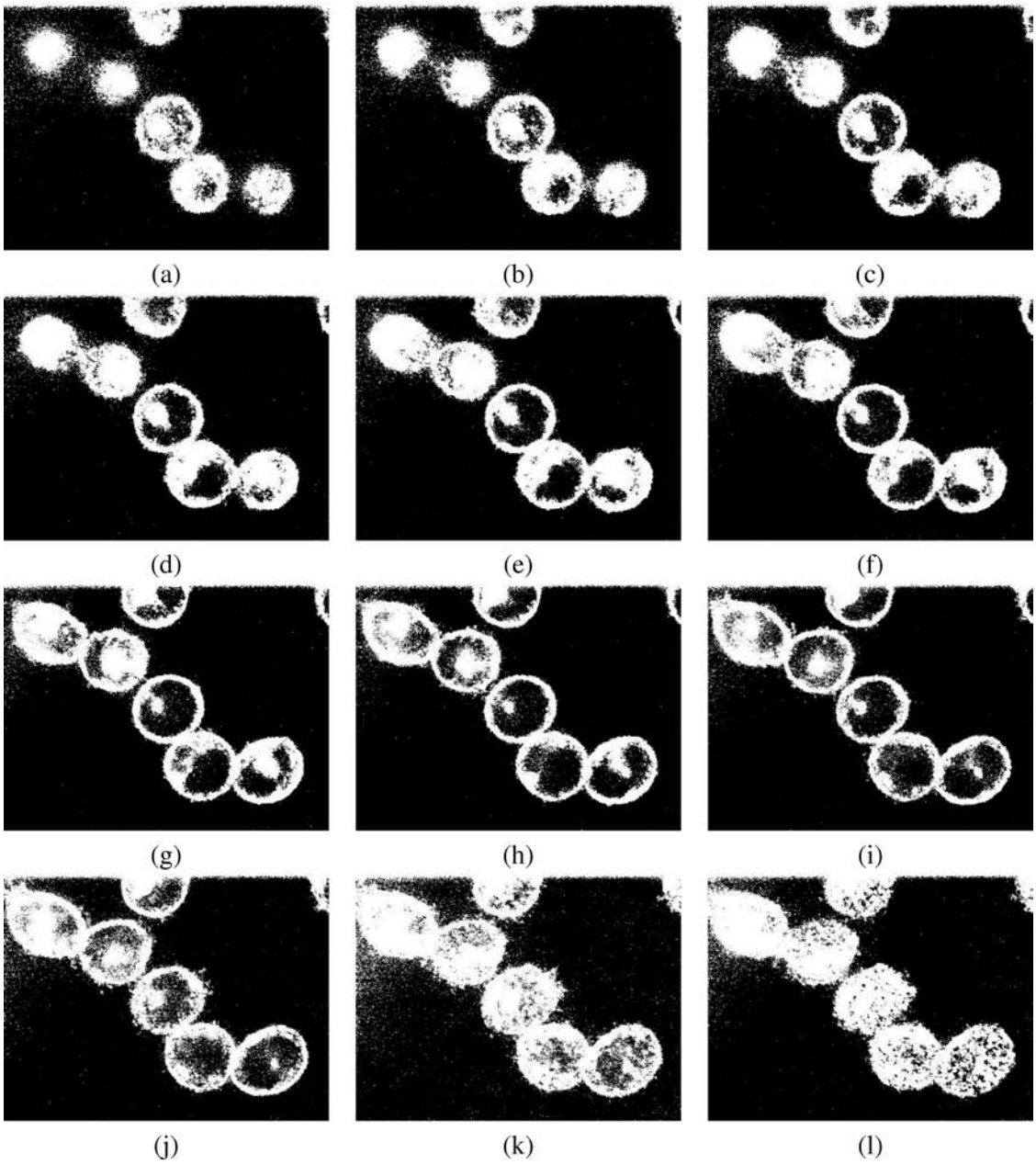

Fig. 3. Sequence 1: Foreground membership probability for optical sections at time $t = 1$ (Bright regions denote higher foreground membership probability and dark regions denote higher background membership probability).

image data is modelled as a two-component GMM. Based on the assumption that the loss of intensity increases relatively with time or depth or both, the first image of the time series or the first z-slice of the stack will have minimal loss of intensity and can be considered as the reference image. The reference image should have good visual information of the object or specimen to be studied. Initially, mean intensity and standard deviation for the foreground and background are estimated with EM algorithm. Then the parameters of the foreground component are used to warp each pixel of the image to its relative reference intensity. Following subsections explain individual steps taken during this process in detail.

Parameter estimation

For a two component GMM of the jth image in a stack, there are six unknown parameters,

$$\theta^j = \left\{ \left(w_1^j, \mu_1^j, \sigma_1^j\right), \left(w_2^j, \mu_2^j, \sigma_2^j\right) \right\}, \tag{1}$$

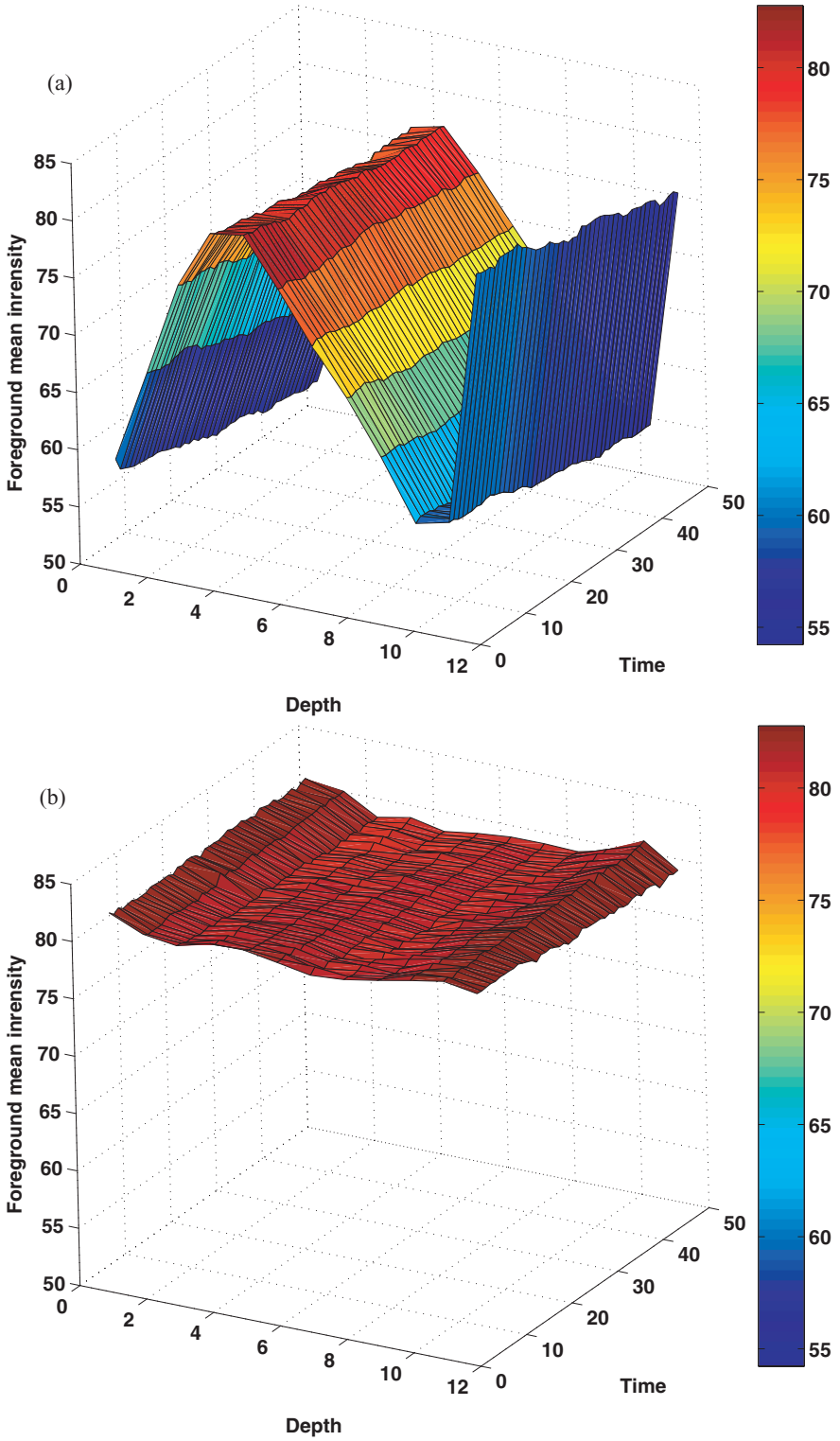

Fig. 4. Sequence 1: Mean intensity of foreground region in (a) original image stack and (b) restored image stack.

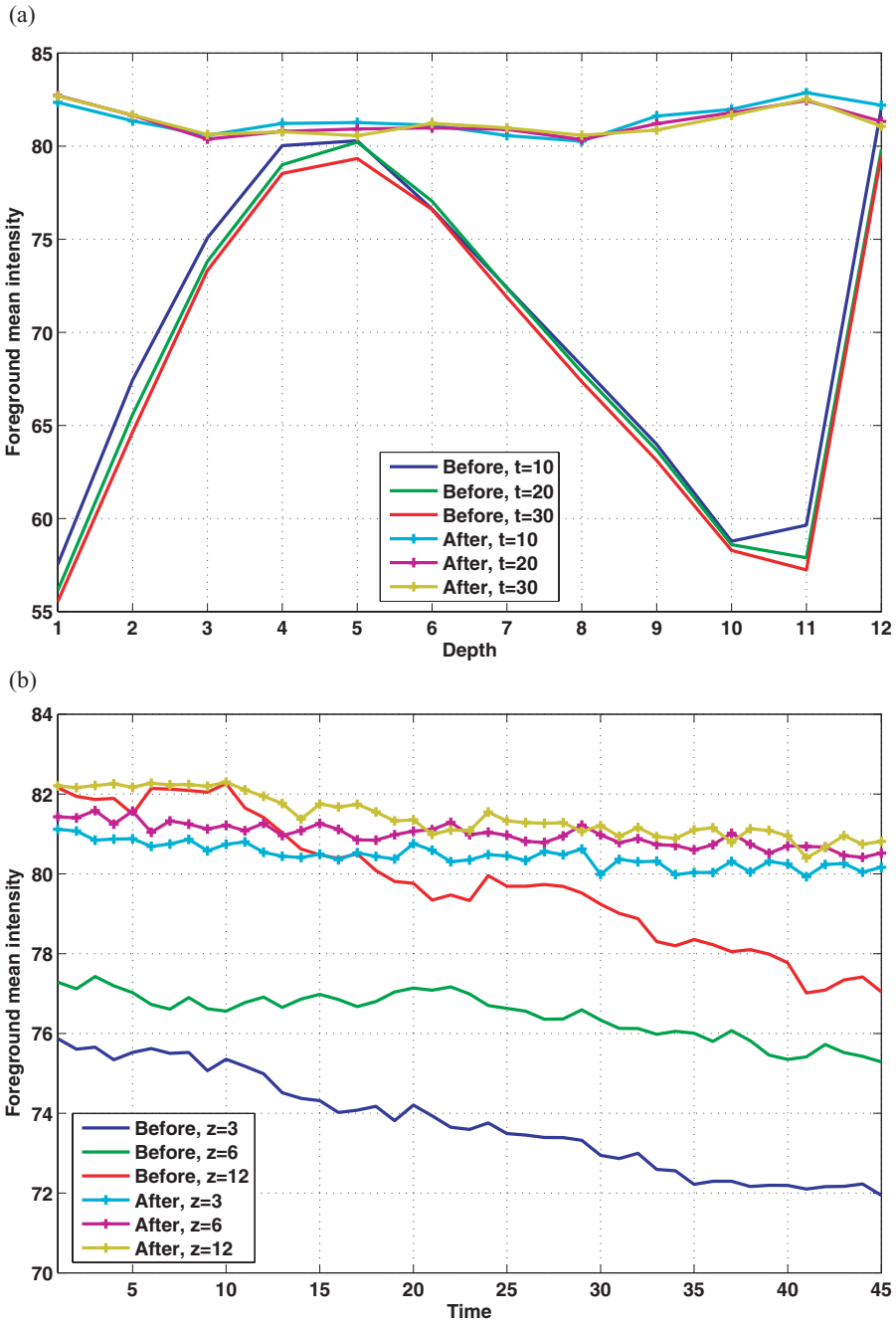

Fig. 5. Sequence 1: Variation in the mean intensity of foreground region of original image stack and restored image stack (a) with depth (b) with time.

where w_1^j, w_2^j are mixture weight constants, μ_1^j, μ_2^j represent mean intensities and σ_1^j, σ_2^j give the standard deviations corresponding to background and foreground Gaussian PDF, respectively, for the jth image. The first step is to estimate the membership probability for each nth pixel of jth confocal microscopy image. Given intensity for this pixel is x_n^j, the membership probability can be calculated as,

$$F_i^j(n) = \frac{w_i^j \cdot P_i^j\left(x_n^j\right)}{w_1^j \cdot P_1^j\left(x_n^j\right) + w_2^j \cdot P_2^j\left(x_n^j\right)}, \tag{2}$$

where

$$P_i^j\left(x_n^j\right) = \frac{1}{\sigma_i^j\sqrt{2\pi}} \exp\left\{\frac{-\left(x_n^j - \mu_i^j\right)^2}{2\left(\sigma_i^j\right)^2}\right\}. \tag{3}$$

In the above equations, $i = 1, 2$ and $n = 1, 2, \ldots, N \times M$, where $N \times M$ is the dimension of the image and $j = 1, 2, \ldots, K$ with K being the number of the image slices. In the second step, the Gaussian PDF mixture parameter values are estimated from the above membership probability:

$$w_i^j = \frac{1}{M \times N} \sum_{n=1}^{M \times N} F_i^j(n), \tag{4}$$

$$\mu_i^j = \frac{\sum_{n=1}^{M \times N} F_i^j(n) \cdot x_n^j}{\sum_{n=1}^{M \times N} F_i^j(n)}, \tag{5}$$

$$\sigma_i^j = \sqrt{\frac{\sum_{n=1}^{M \times N} F_i^j(n) \cdot (x_n^j - \mu_i^j)^2}{\sum_{n=1}^{M \times N} F_i^j(n)}}. \tag{6}$$

The above two steps are iterated until all the parameters converge. The iterative process is repeated for each image in the stack.

Image warping

Once the mixture parameters for the image are known, intensity can be compensated by compensating these parameters to match some reference. The compensated intensity for the nth pixel in the jth image can be calculated from original intensity x_n^j as:

$$(x')_n^j = F_2^j(n) \cdot \left\{ \frac{(x_n^j - \mu_2^j)}{\sigma_2^j} \sigma_r + \mu_r \right\} + F_1^j(n) \cdot x_n^j. \tag{7}$$

Here, μ_r and σ_r represent mean and standard deviation references for the foreground. Mean and standard deviation of the first image in the stack can be set as the reference parameters for the image stack restoration. However, in the case where the first image in the stack does not have enough details or is not the brightest, one of the other images can be chosen to be the reference. Figure 1 summarizes the entire compensation algorithm.

Experimental results

The proposed approach was implemented in MATLAB and was tested on several sets of images in the Biovision lab database at University of Texas at Arlington. Before proceeding to the experimental results, we will briefly talk about the initialization used for the experiment. Initialization is crucial for the EM algorithm. As parameters from the reference frame are needed for image restoration, EM is carried out on the reference image first. The mixture weights for the reference frame m can be initialized as

$$w_1^m = w_1^m = 0.5.$$

Since the background mean is lower than the overall image mean and foreground mean is higher, one can select the initial values arbitrarily to follow this restriction,

$$\mu = \frac{1}{M \times N} \sum_{n=1}^{M \times N} x_n^m, \mu_1^m = \frac{\mu}{2}, \mu_2^m = \frac{3\mu}{2}.$$

A good initial value for the mixture standard deviation is the overall standard deviation of the image.

$$\sigma_1^m = \sigma_2^m = \sqrt{\frac{1}{(M \times N) - 1} \sum_{n=1}^{M \times N} (x_n^m - \mu)^2}.$$

These values can be improved upon by randomly using various initializations and then choosing the one that maximizes the membership probabilities. However, reasonable fixed values as stated above were used for the repeatability of the experiment. After successful completion of the EM procedure for reference frame m, reference parameters are set as

$$\mu_r = \mu_2^r, \sigma_r = \sigma_2^r.$$

As any image in the sequence is very similar to its previous image, the parameters of the previous image after EM are used to initialize the EM procedure for the next image.

$$w_1^j = w_1^{j-1}, \mu_1^j = \mu_1^{j-1}, \sigma_1^j = \sigma_1^{j-1},$$

$$w_2^j = w_2^{j-1}, \mu_2^j = \mu_2^{j-1}, \sigma_2^j = \sigma_2^{j-1}.$$

This initialization also helps to reduce the computational burden by reducing the number of EM iterations. MATLAB implementation of the proposed method with above initialization takes less than 1 s per optical section on an average on a 2.53 GHz Pentium 4 computer. This is faster compared to Ĉapek *et al.* (2006), who report that C++ implementation of their approach takes approximately 2 s per optical section. A C++ implementation of our approach can provide further speed-up if needed.

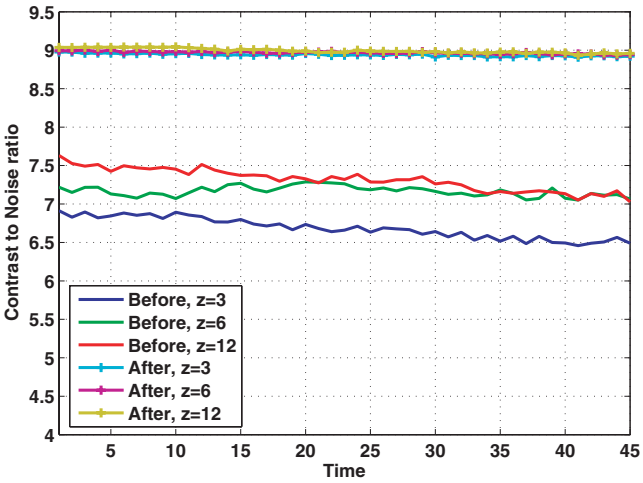

Fig. 6. Sequence 1: Contrast-to-noise ratio.

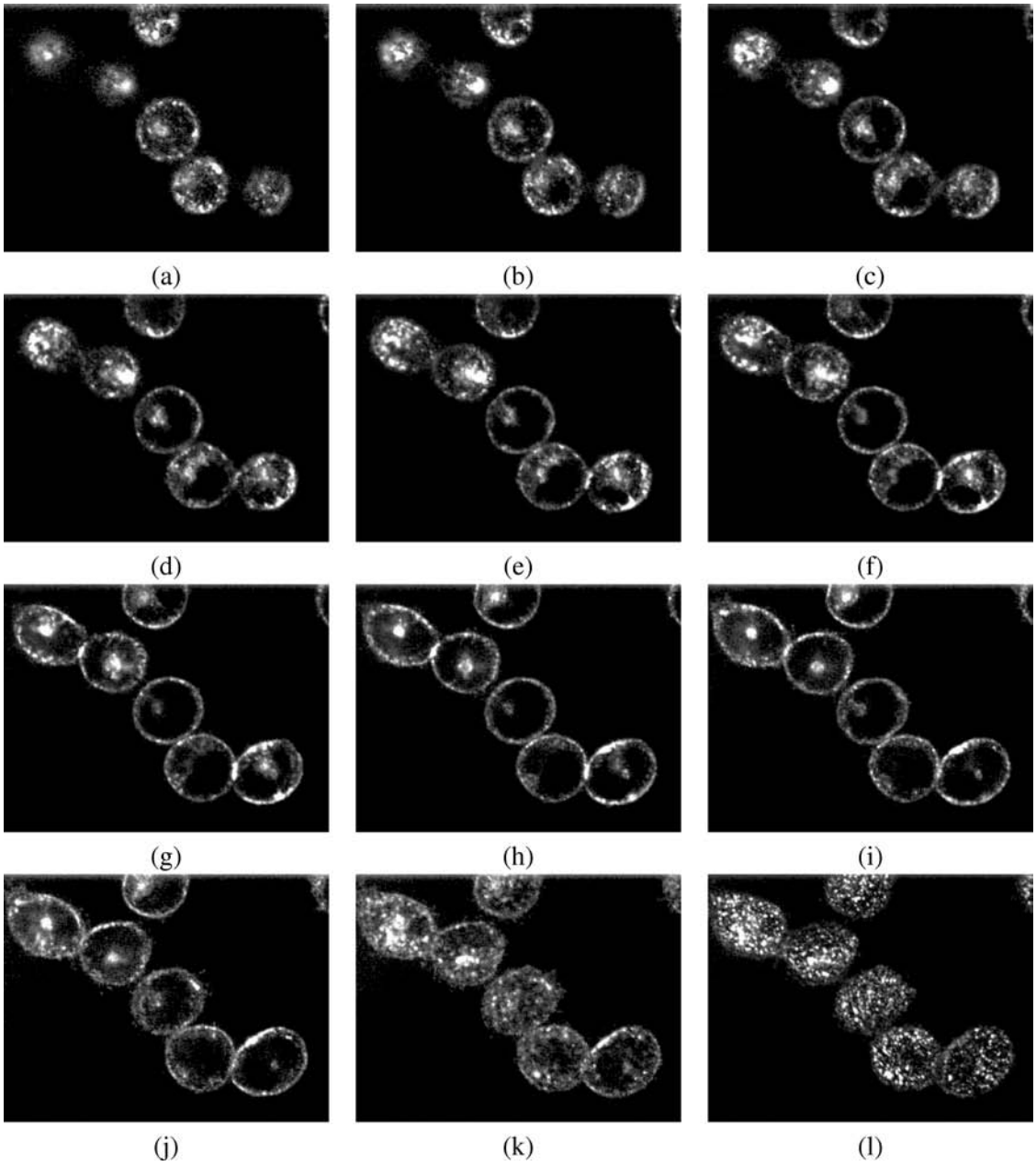

Fig. 7. Sequence 1: Restored optical sections at time $t = 1$ from (a) top ($z = 1$) to (l) bottom ($z = 12$).

Sequence 1

The sequence tested here is a 4D-*xyzt* sequence with resolution $336 \times 256 \times 12 \times 45$ acquired by spinning disk confocal microscopy, and showing the trafficking of caveolin1-GFP in a CHO (Chinese hamster ovary) cell. Figures 2(a) to (l) show all the 12 optical sections at time $t = 1$. It can be observed from the images that the intensity of the optical sections varies significantly from one section to the other. The intensity rises from depth $z = 1$ to $z = 5$ and drops again till $z = 11$ before it rises in the final optical section at $z = 12$. These intensity changes primarily result from a combination of increasing z depth, changes in cross-sectional area of the cell, and actual changes in the distribution of caveolin1-GFP, which is concentrated on the cell surface relative to the cell interior. Section 12 shows the bottom surface of the cell where it is spread out on the glass cover slip. The top surface of the cell was not included in the z stack. In addition, the morphology of discrete fluorescent objects changes with the depth. GMM parameters were calculated with EM algorithm. For each frame, the iterative process was terminated when foreground and background mean values changed by less than 0.01.

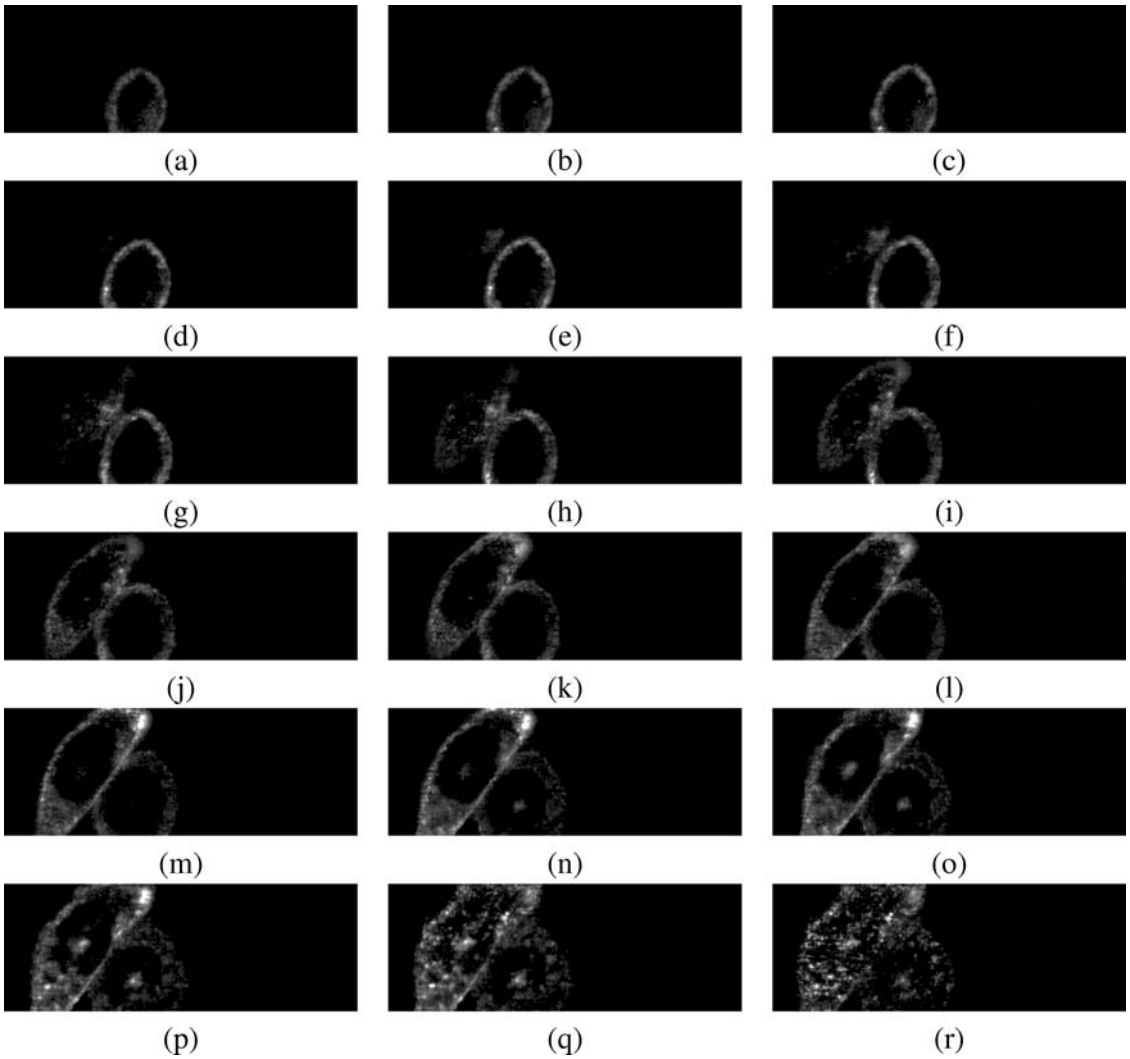

Fig. 8. Sequence 2: Original image stack: optical sections from $z = 1$ to 18, at $t = 30$.

Figure 3 shows the foreground membership probability after the convergence of EM algorithm. Since these are membership probabilities and not memberships, these can take any value from 0 to 1. The brightness of a pixel is higher, that is the probability is close to one, if it belongs to the foreground. On the other hand, the darkness of a pixel indicates that it belongs to background (this means the probability is close to 0). Despite the structural changes and changes in intensity,

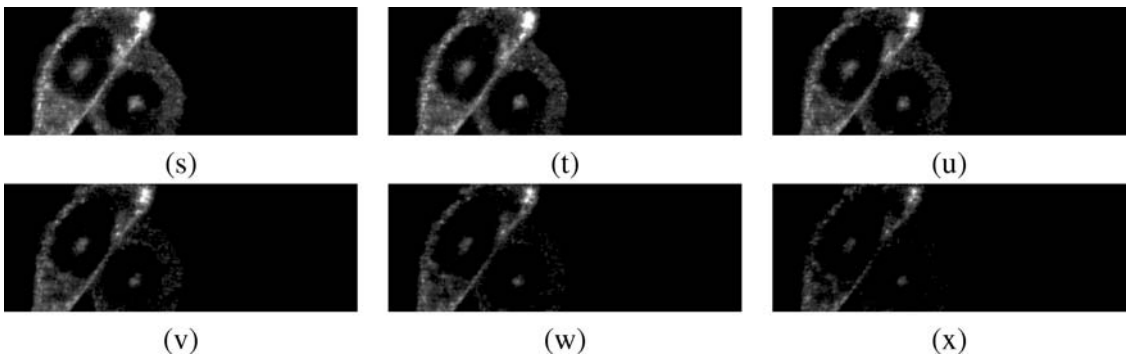

Fig. 9. Sequence 2: Original image stack: optical sections at $z = 15$ for $t = 1, 12, 24, 36, 48, 60$.

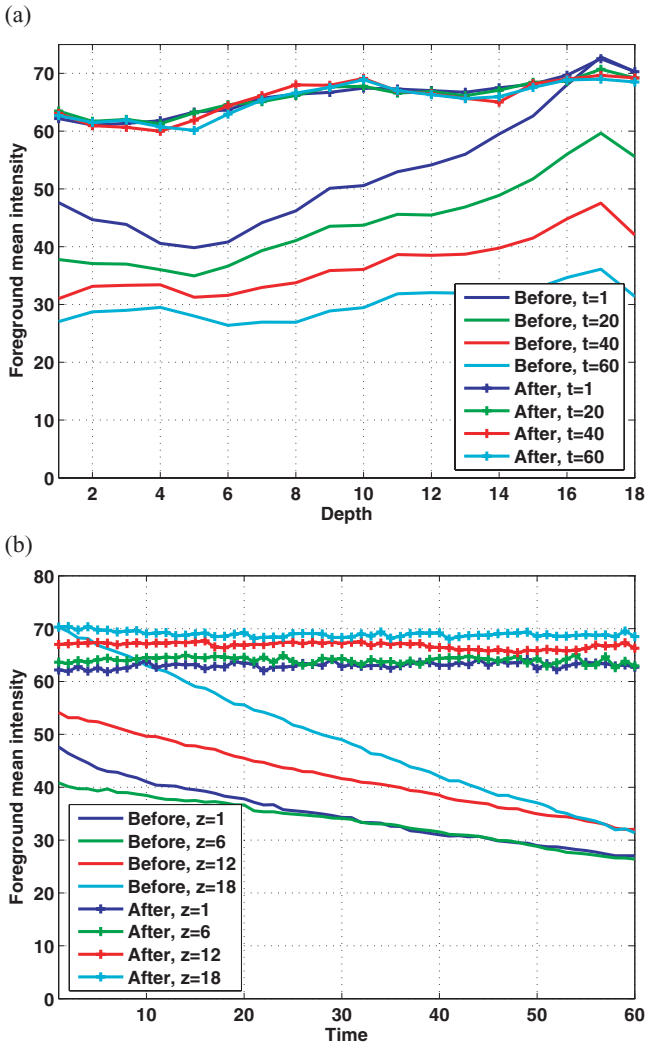

Fig. 10. Sequence 2: Variation in the mean intensity of foreground region of original image stack and restored image stack (a) with depth (b) with time.

the foreground regions are consistently detected. The success of the proposed method can be attributed to this consistency. Figure 4 shows foreground mean intensities for the entire image stack before and after compensation. A few of the curves are extracted in Fig. 5 to observe the intensity loss trends closely. Figure 5(a) shows the plot for the variation in the foreground mean with depth at time t =10, 20, 30, which is in agreement with the visual observations made. However, variation of mean intensity with time plotted in Fig. 5(b) for depth $z = 3, 6, 12$ reveal facts that are difficult to observe visually. Intensity of the foreground drops as the time progresses as expected owing to effects of photobleaching. However, rate of the decay is different at different depth levels. At depth $z = 6$, the mean intensity drops from 77.3 to 75.3, whereas at depth $z = 12$ it drops from 82.2 to 77.0. Decay rate at $z = 12$ is more than two times the decay rate at $z = 6$. As

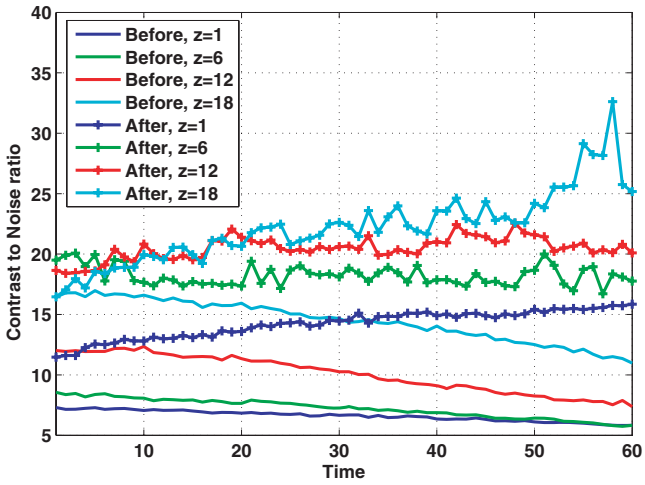

Fig. 11. Sequence 2: Contrast-to-noise ratio.

our method does not use IDF, estimation of complicated IDF required to model this image sequence becomes unnecessary. The image sequence was restored with reference values $\mu_r = 82.2$ and $\sigma_r = 50.9$, which were estimated from frame at $t = 1$ and $z = 12$. This frame was chosen as it has the maximum mean intensity. Restored images at $z = 1$ are shown in Fig. 7. Foreground intensities of the restored image stacks are plotted in Fig. 4(b). Steady values of the intensities can be observed in the plot. The steady values are also reflected in the restored images in Fig. 7. Contrast-to-noise ratio (CNR) was computed for the sequence for quantitative analysis.

$$\mathrm{CNR} = \frac{\mu_2^j - \mu_1^j}{\sigma_1^j}. \tag{8}$$

Figure 6 shows CNR curves before and after compensation for depths $z = 3, 6, 12$. A substantial increase in the CNR after the compensation can be seen for all the depths.

Sequence 2

The next sequence is a 4D-*xyzt* sequence similar to the first sequence with resolution $333 \times 120 \times 18 \times 60$. Compared to the first sequence, the second sequence shows more structural changes as seen in Fig. 8. The shape of the foreground object changes from a single round object in the top optical section to the two elongated objects in the deeper optical sections. It also exhibits severe photobleaching with time (Fig. 9). Foreground mean intensities are dropping drastically with time as seen in Fig. 10(b). Worst drop is from 70.3 to 31.4 at depth $z = 18$. Although, the least drop is experienced by $z = 6$, it has the least foreground mean intensity to start with. The sequence was restored by selecting optical section at $z = 18$ at time $t = 1$ with $\mu_r = 70.3$ and $\sigma_r = 43.6$. Steady intensities can be seen after the restoration in Figs 12, 13 and also in 10 (a) and 10 (b). CNR for this sequence is shown in Fig. 11.

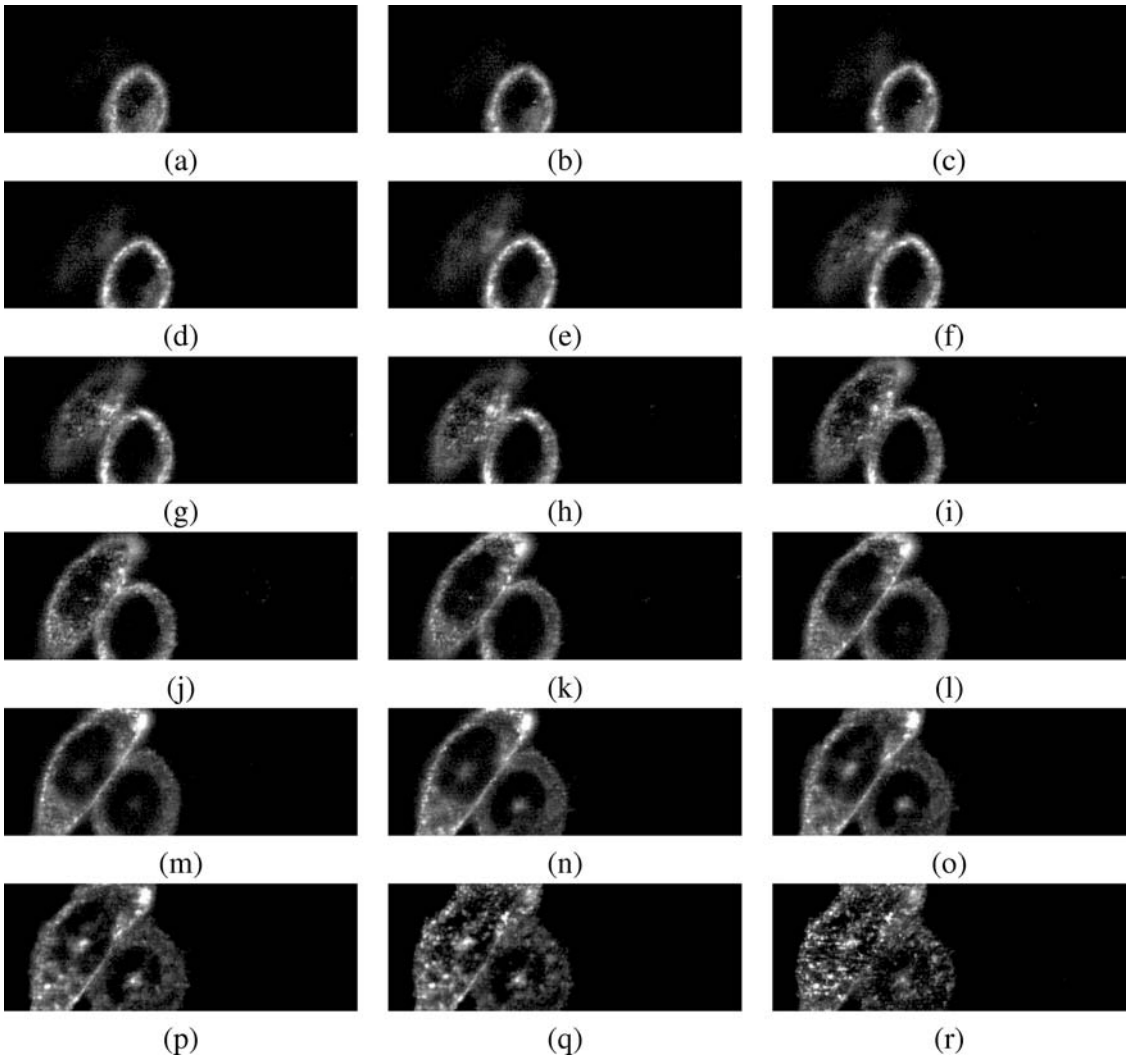

Fig. 12. Sequence 2: Restored image stack: optical sections from $z = 1$–18, at $t = 30$.

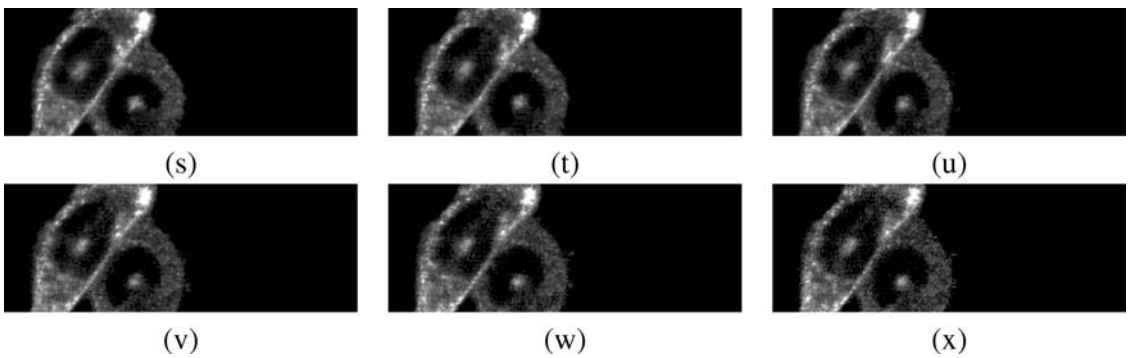

Fig. 13. Sequence 2: Restored image stack: optical sections at $z = 15$ for $t = 1, 12, 24, 36, 48, 60$.

Sequence 3

The third image sequence is a 3D-*xyt* sequence of dimensions $512 \times 512 \times 220$ showing trafficking of caveolin1-GFP in a single optical section. For this long sequence, intensity loss due to photobleaching is prominent as frame number increases. Mean intensity of the foreground drops from 35 to 21.5 from frame at time $t = 1$ to $t = 220$. Changes of object shape

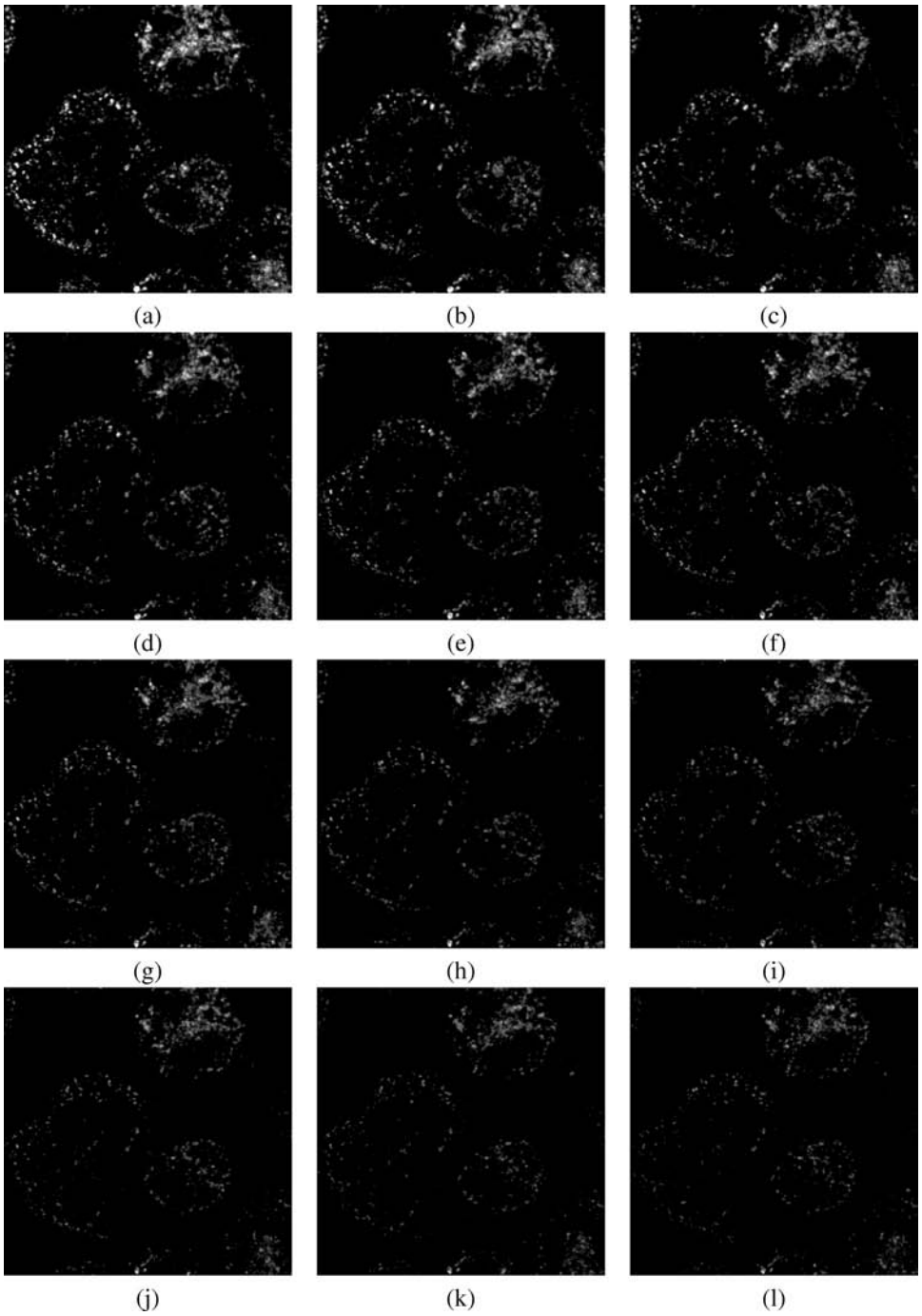

Fig. 14. Sequence 3: Reference section $t = 1$ and some sections from an original image stack. Sections: (a) $t = 1$, (b) $t = 20$, (c) $t = 40$, (d) $t = 60$, (e) $t = 80$, (f) $t = 100$, (g) $t = 120$, (h) $t = 140$, (i) $t = 160$, (j) $t = 180$, (k) $t = 200$, (l) $t = 220$.

from frame to frame are mainly due to object motion, and are minimal compared with those resulting from changing optical section as in the first two sequences. In Fig. 14, we show the few images from the original sequence of confocal microscopy images. The entire sequence was processed by our algorithm using first frame (Fig. 14(a)) as the reference image. Reference values were $\mu_r = 34.7$ and $\sigma_r = 36.8$. From Fig. 16, one can see that the intensity drops steadily with increasing time-point. Generally, this decay is modelled with an IDF. A simple photophysical model for photobleaching is a single exponential decay, but the actual IDF may be much more complicated and impossible to estimate *a priori*. The proposed

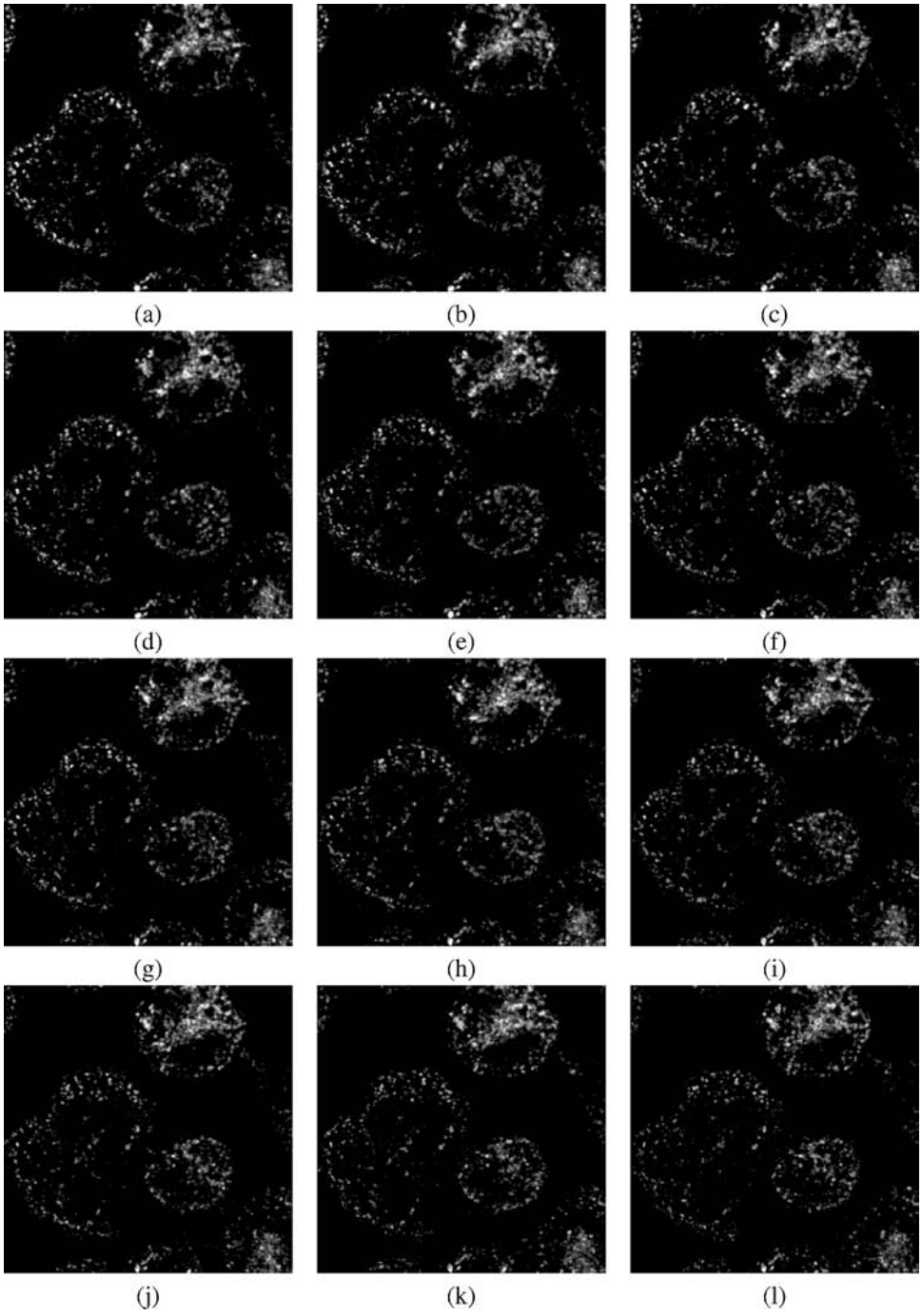

Fig. 15. Sequence 3: Reference section $t = 1$ and some sections from restored image stack. Sections: (a) $t = 1$, (b) $t = 20$, (c) $t = 40$, (d) $t = 60$ (e) $t = 80$, (f) $t = 100$, (g) $t = 120$, (h) $t = 140$, (i) $t = 160$, (j) $t = 180$, (k) $t = 200$, (l) $t = 220$.

method has helped to maintain a constant intensity for the entire stack after the compensation without any IDF. In Figs 15 and 16, it can be observed that the intensities of the foreground object of the restored series are uniform with very little variation. For the first frame, the number of iterations taken for EM to converge was 63. For the rest of the frames, it required only 1.36 iterations on average, with a minimum of 1 and a maximum of 11 iterations. Thus, using previous frames estimated parameters to initialize the next frames' parameters helps to reduce computational load significantly. Fig. 17 shows CNR before and after compensation.

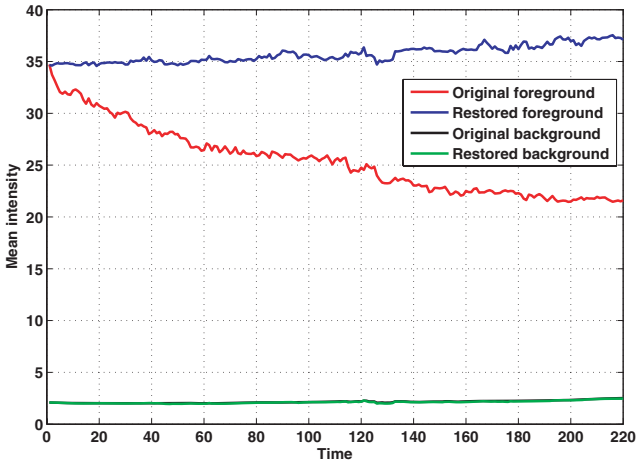

Fig. 16. Sequence 3: Mean intensity of background and foreground.

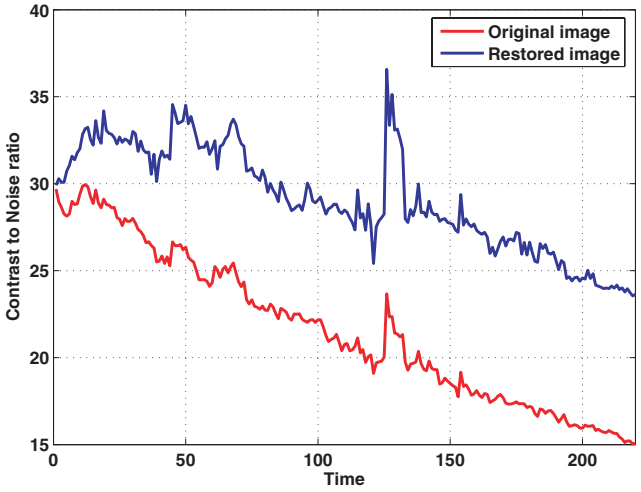

Fig. 17. Sequence 3: Contrast-to-noise ratio.

Sequence 4

Sequence 4 is a 3D-*xyt* sequence similar to Sequence 3 with resolution 512 × 512 × 166. For this image sequence, it is difficult to separate the foreground and background visually. Foreground membership probability for the optical sections shown in Fig. 18 are depicted in Fig. 19 as estimated by the proposed algorithm. Similar to sequence 3, Fig. 21 shows the decay of foreground intensity over time. The first frame of the sequence was chosen as the reference frame. Reference mean μ_r was calculated to be 35.4 and reference standard deviation σ_r was 27.1. Restored images are shown in Fig. 20 and corresponding contrast-to-noise ratios are plotted in Fig. 22.

Conclusion

For reliable analysis as well as visualization of cell dynamics, it is essential that the acquired images reflect the exact information of the specimen. The objective of the proposed method was to help regain the visual information lost due to various deteriorating factors such as scattering and absorption of the excitation, photobleaching of fluorescent images etc. Majority of the current approaches to solve this problem are either computationally complex, time-consuming, restricted to parametric decay models (IDF) or are highly sensitive to noise. The proposed method provides a simple yet effective statistical approach to solve this problem. It overcame the disadvantages of current methods and at the same time increased the visual value of confocal microscopy images. The main idea was to filter the foreground information from a given image by modelling it as a mixture of Gaussian PDFs and use this information to compensate the intensity loss of the confocal microscopy images. When multiple fluorescence tags are used in a specimen, the proposed method can be simply applied to the individual tags or a multiple Gaussian PDF mixture model can be used to handle the scenario.

References

Atkins, P. & De Paula, J. (1994) Spectroscopy 2: electronic transitions. *Physical Chemistry*, pp. 590–622. W.H. Freeman and Company, New York.

Becker, P.L. (1996) Quantitative fluorescence measurements. *Fluorescence Imaging Spectroscopy and Microscopy* (ed. by Wang, X.F. & Herman, B.), pp. 1–29. Wiley, New York.

Ĉapek, M., Janàĉek, J. & Kubínová, L. (2006) Methods for compensation of light attenuation with depth of images captured by a confocal microscope. *Micros. Res. Tech.* **69**, 624–635.

Ĉapek, M., Kubínová, L., Hána, K. & Smrĉka, P. (2005) Compensation of the contrast and brightness attenuation with depth in confocal microscopy. In *Proceedings of the Spring Conference on Computer Graphics 2005*, 225–228.

Chen, H., Swedlow, J.R., Grote, M., Sedat, J.W. & Agard, D.A. (1995) The collection, processing, and display of digital three-dimensional images of biological specimens. *Handbook of Biological Confocal Microscopy* (ed. by Pawley, J.B.), pp. 197–210. Plenum Press, New York.

Cox, I., Roy, S. & Hingorani, S. (1995) Dynamic histogram warping of image pairs for constant image brightness. In *Proceedings of the IEEE International Conference on Image Processing 1995*, **2**, 366–369.

Kervrann, C., Legland, D. & Pardini, L. (2004) Robust incremental compensation of the light attenuation with depth in 3D fluorescence microscopy. *J. Microsc.* **214**(3), 297–314.

Negahdaripour, S. & Yu, C.-H. (1993) A generalized brightness change model for computing optical flow. In *Proceedings of the IEEE International Conference on Computer Vision 1993*, 2–11.

Nyul, L., Udupa, J. & Zhang, X. (2000) New variants of a method of MRI scale standardization. *IEEE Trans. Med. Img.* **19**(2), 143–150.

Oostveldt, P.V., Verhaegen, F. & Messens, K. (1998) Heterogeneous photobleaching in confocal microscopy caused by differences in refractive index and excitation mode. *Cytometry* **32**, 137–146.

Ortiz, S., Garcia, E., Jones, A., Pinkel, D., Gray, J., Sudar, D. & Lockett, S. (1999) Segmentation of confocal microscope images of cell nuclei in thick tissue sections. *J. Microsc.* **193**, 212–2266.

Periaswamy, S. & Farid, H. (2003) Elastic registration in the presence of intensity variations. *IEEE Trans. Med. Imag.* **22**(7), 865–874.

Rigaut, J. & Vassy, J. (1991) High-resolution 3D images from confocal scanning laser microscopy: quantitative study and mathematical correction of the effects from bleaching and fluorescence attenuation in depth. *Anal. Quant. Cytol.* **13**, 223–232.

Song, L., Varma, C.A., Verhoeven, J.W. & Tanke, H.J. (1996) Influence of the triplet excited state on the photobleaching kinetics of fluorescein in microscopy. *Biophysics* **70**, 2959–2968.

Theodoridis, S. & Koutroumbas, K. (1999) *Pattern Recognition*. Academic press, San Diego.

Wu, H.-X. & Ji, L. (2005) Fully automated intensity compensation for confocal microscopic images. *J. Microsc.* **220**(1), 9–19.

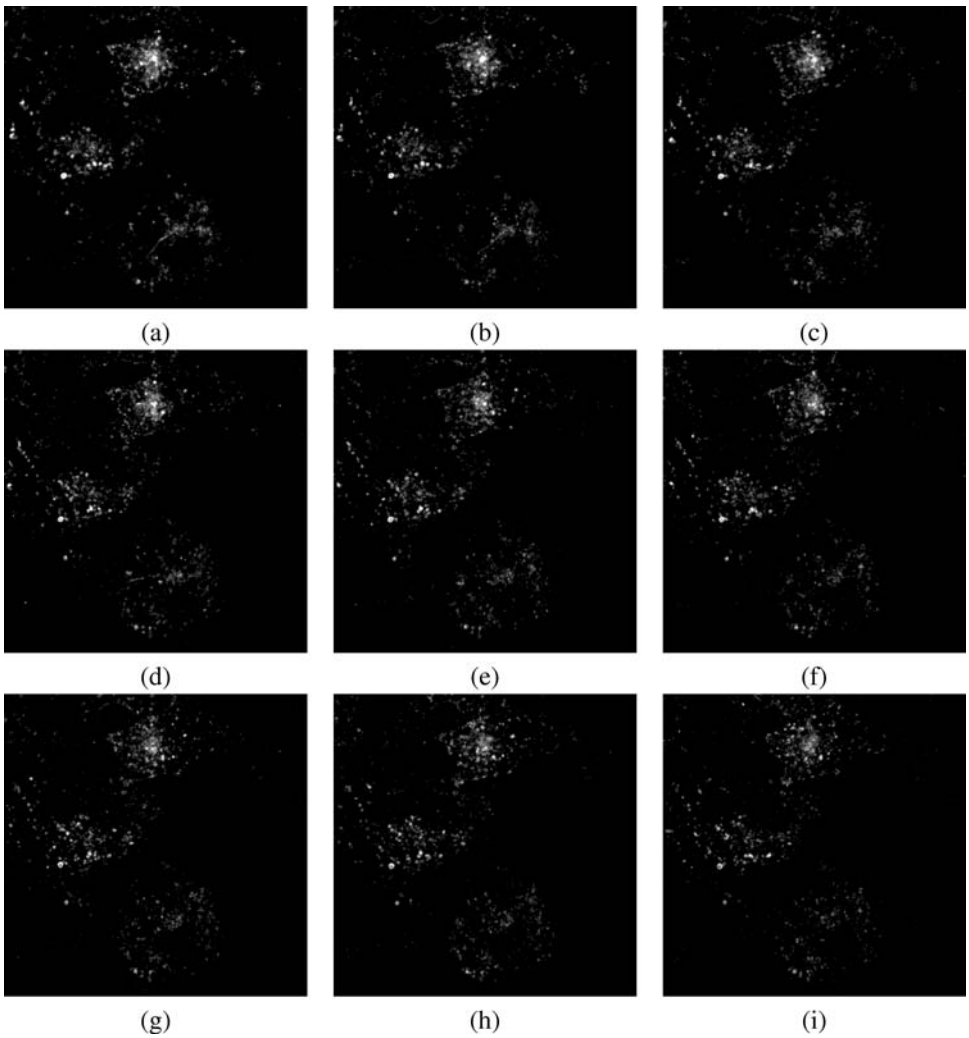

Fig. 18. Sequence 4: Reference section $t = 1$ and some sections from original image stack. Sections: (a) $t = 1$, (b) $t = 20$, (c) $t = 40$, (d) $t = 60$, (e) $t = 80$, (f) $t = 100$, (g) $t = 115$, (h) $t = 130$, (i) $t = 166$.

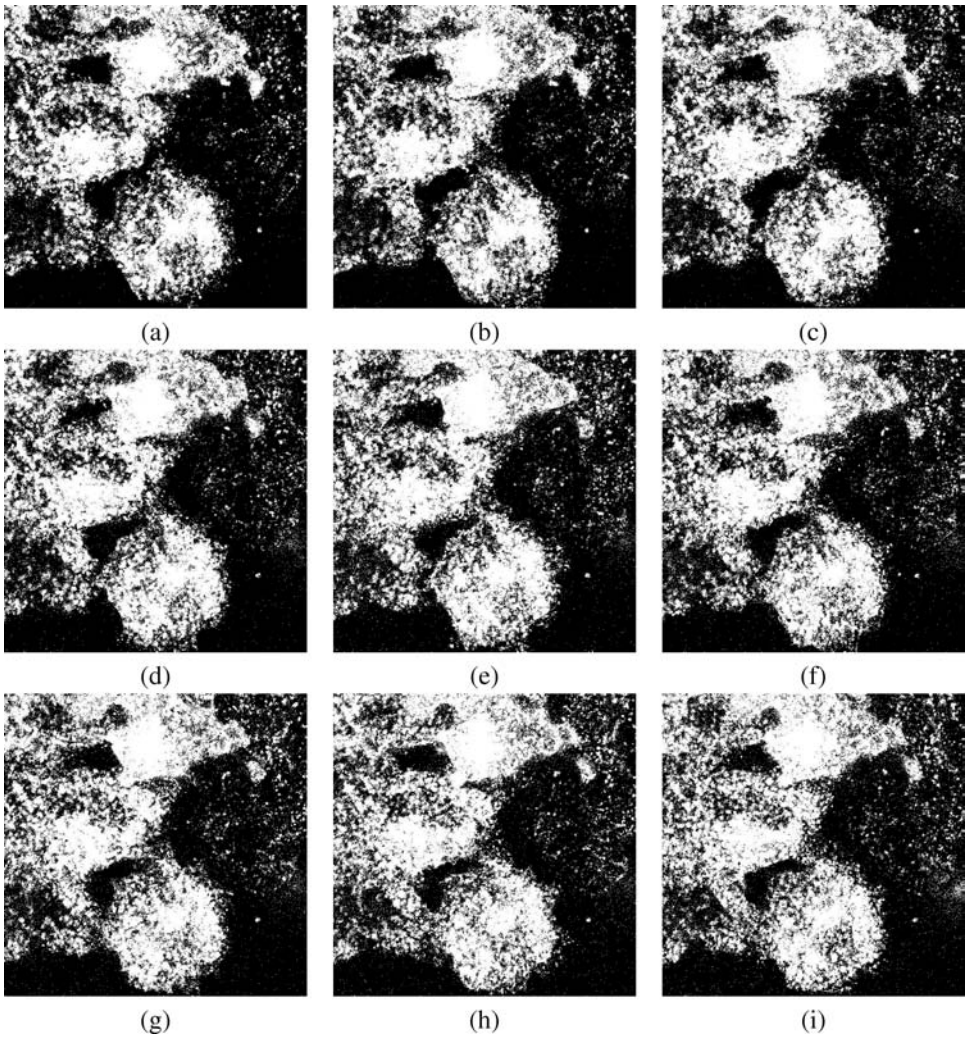

Fig. 19. Sequence 4: Foreground membership probability for optical sections at time (a) $t = 1$, (b) $t = 20$, (c) $t = 40$, (d) $t = 60$, (e) $t = 80$, (f) $t = 100$, (g) $t = 115$, (h) $t = 130$, (i) $t = 166$ (Bright regions denote higher foreground membership probability and dark regions denote higher background membership probability).

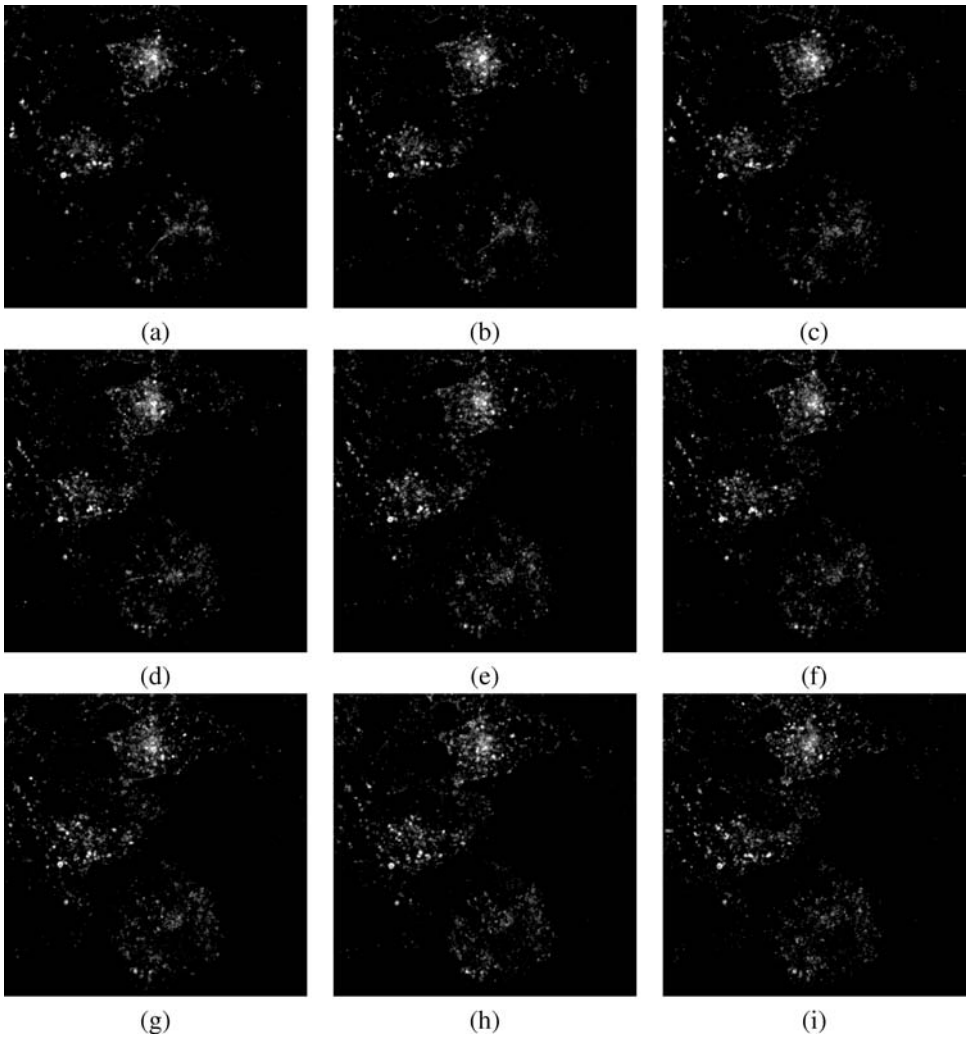

Fig. 20. Sequence 4: Reference section $t = 1$ and some sections from restored image stack. Sections: (a) $t = 1$, (b) $t = 20$, (c) $t = 40$, (d) $t = 60$, (e) $t = 80$, (f) $t = 100$, (g) $t = 115$, (h) $t = 130$, (i) $t = 166$.

